2024 IEEE/OES Thirteenth Current, Waves and Turbulence Measurement (CWTM) | 979-8-3503-9391-0/24/$31.00 ©2024 IEEE | DOI: 10.1109/CWTM61020.2024.10526345

Measuring turbulence from wave-following platforms

Kristin Zeiden
Applied Physics Laboratory
University of Washington
Seattle, United States
kzeiden@uw.edu

Jim Thomson
Applied Physics Laboratory
University of Washington
Seattle, United States
jthomson@apl.washington.edu

***Abstract*—Autonomous surface platforms equipped with pulse-coherent high-resolution (HR) ADCPs are a promising tool for measuring turbulence and estimating turbulent dissipation rates, $\epsilon(z)$, close to the air-sea interface. However, surface gravity waves generate significant bias in $\epsilon(z)$ if not sufficiently separated from the turbulent signal. In a previous study, the authors developed a method of isolating wave orbital velocities from the data using empirical orthogonal functions (EOFs). Low-mode EOFs had characteristics of surface gravity waves, while higher-mode EOFs had characteristics of turbulence. After filtering empirical wave profiles constructed from the low-mode EOFs from the data, resultant $\epsilon(z)$ were in close agreement with law-of-the-wall scaling during quiescent conditions. In this study, we further validate the EOF-filtering technique by comparing EOFs of the HR ADCP data with those computed from synthetic wave data which does not contain turbulence. As expected, low-mode EOFs of the synthetic data are in strong agreement with those of the real data, while high-mode EOFs reflect only noise due to the absence of turbulence. Wave profiles constructed from the low-mode EOFs are then used to quantify the potential for bias in $\epsilon(z)$ if wave velocities are not sufficiently filtered from the data.**

***Index Terms*—Ocean, turbulence, waves, dissipation, drifters**

I. Introduction

The proliferation of Lagrangian surface platforms combined with recent improvements in pulse-coherent, high-resolution acoustic Doppler current profilers (HR ADCPs) have enabled robust measurements of fine-scale turbulent velocities in the near surface across an increasingly wide range of forcing conditions and geographic locations. HR ADCP data is ideal for estimating the turbulent kinetic energy dissipation rate near the surface, $\epsilon(z)$, as it measures the spatial structure of turbulent velocities directly. However, strong shear associated with surface gravity waves can lead to dissipation rate estimates which are biased high [1].

Recently, [2] developed an empirical method of filtering wave orbital velocities from HR ADCP data via empirical orthogonal function (EOF) analysis. The method was developed using turbulence data predominantly obtained with HR ADCPs mounted on 'Surface Wave Instrument Floats with Tracking' (SWIFTs, Figure 1) [3]. The authors demonstrated that low-mode EOFs of the data had characteristics expected of surface gravity waves, while higher-mode EOFs had characteristics of turbulence. Estimates of $\epsilon(z)$ from an example ADCP burst filtered using the EOF method were in close agreement with law-of-the-wall scaling from concurrent measurements of surface wind speed.

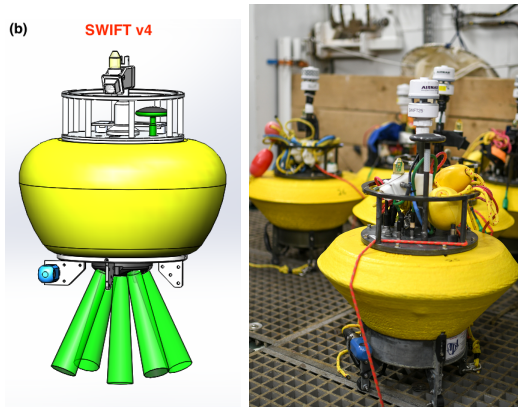

Fig. 1. Version 4 SWIFT drifters (left) schematic and (right) being prepped for deployment. A Nortek Signature1000 HR ADCP is mounted at the base of the float in a downlooking configuration. The five beams of the ADCP are illustrated in green. Graphic courtesy of Joe Talbert and Alex DeKlerk, image courtesy of Kerstin Bergentz.

Here we present new work to further validate the EOF-filtering technique of [2]. We compare EOFs of the ADCP data with those of synthetic velocity data characterized by broad-band surface gravity waves and no turbulence. As expected, low-mode (high energy) EOFs of the synthetic data exhibit characteristics of surface gravity waves and closely resemble the same EOFs of the real data, while higher-mode (lower energy) EOFs have characteristics of noise. Unlike EOFs of the real data, characteristics of inertial subrange turbulence are absent from these synthetic EOFs. Finally, we demonstrate the efficacy of the method with new results showing $\epsilon(z)$ measured during a strong storm is in strong agreement with law-of-the-wall scaling predictions.

II. Methods

A. Structure Function Method

An advantage of HR ADCP data is that $\epsilon(z)$ may be estimated from the fine-scale spatial structure of velocity

directly [4]. Kolmogorov theory gives a simple scaling for the TKE dissipation rate in the inertial subrange,

$$\epsilon \propto u(r)^3/r \tag{1}$$

where $u(r)$ is the velocity associated with turbulent eddies at scale r. Dissipation rate at a given location along a path (here depth, z) may then be related to the second order velocity structure function, $D(z,r) = [u(z+r/2) - u(z-r/2)]^2$, by

$$D(z,r) = C_\nu^2 \epsilon(z)^{2/3} r^{2/3} \tag{2}$$

where C_ν^2 is a constant empirically determined to be 2.1 [5]. The method is then to fit measurements of D at a given depth and computed over a range of separation scales to the model $D(z,r) = Ar^{2/3} + N$, where the offset N is proportional to the instrument noise. The model fit then gives $\epsilon(z) = [A(z)/C_\nu^2]^{3/2}$. Further details of the application of the method are given in [2].

B. EOF Filtering

The challenge inherent to the structure function method is to remove non-turbulent shear from the data prior to computing $D(z,r)$. Near the surface, this means isolating turbulence from surface waves, which cannot be easily separated by time-averaging the data. EOFs are well suited to capture the variance of surface gravity waves, which are coherent in (vertical) space and typically at least an order of magnitude stronger than turbulent velocities. EOFs are eigenfuctions of the data-data covariance matrix, and corresponding eigenvalues give the percentage of total variance contained in each EOF [6]. The time varying amplitude of each EOF is obtained by projecting the eigenfunction back onto the data. In [2] the data-data covariance matrix is taken to be the covariance between the velocity timeseries of each possible ADCP bin pair, e.g. the covariance between $w(z = 1$ m, $t)$ and $w(z = 2$ m, $t)$. EOFs can be interpreted as statistical 'modes' of the data, with the lowest modes (EOFs which contain the most variance) representing time-varying features which have the most energy and greatest coherence across the array, here meaning across ADCP depth bins. Because we expect the signal due to surface gravity waves to be highly coherent across ADCP depth bins and an order of magnitude greater than turbulence, the lowest mode EOFs should contain wave variance only. Filtering these EOFs from the data then in theory removes the contribution to shear from waves.

III. Data

A. SWIFT drifters

Our velocity measurements are collected with SWIFT drifters (Fig. 1). SWIFTs are designed to measure near-surface turbulence in a surface following reference frame [3]. Velocities are measured by HR ADCPs mounted in either an upward or downward looking orientation. SWIFTs are additionally equipped with an inertial motion unit (IMU) and global positioning system (GPS) to measure the surface gravity wave spectrum, a conductivity temperature sensor (CT), and an anemometer to measure wind speed and other atmospheric variables. SWIFTs are typically configured to collect raw data in 8.5 minute 'bursts' every 12 minutes. Preliminary burst-averaged data are telemetered back to a shore-side server via an onboard iridium satellite modem, and raw data are stored in an SD card and offloaded after recovery.

B. HR ADCP Data

The current version SWIFTs (version 4, 'V4') are equipped with a Nortek Signature1000 pulse-coherent HR ADCP [7]. The ADCP emits 1 MHz acoustic pulses at a ping frequency of either 4 or 8 Hz. Velocities are calculated from the doppler shift of the reflected acoustic signal, with range determined by the time gating of the signal. Velocities are measured in 4 cm bins down to a few meters depth, up to 5 m depending on the pulse lag configuration. The SWIFT ADCPs are set to collect data in 8.5 minute bursts, corresponding to at least $\sim$ 4000 pings per burst. Phase ambiguity can occur for relative velocities which exceed a specific known threshold (dependent on the pulse settings), which results in anomalous data spikes [8]. Thus excessive spiking can become a problem in the presence of especially strong velocities. However, Lagrangian platforms are ideal for the use of HR ADCPs as the platform moves with the water and therefore measures relative rather than absolute velocity. Prior to computing dissipation rate, raw ADCP data are quality controlled to remove spikes following [2].

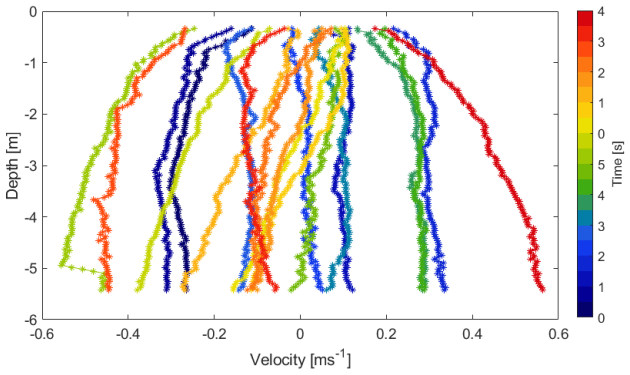

Fig. 2. Profiles of relative velocity obtained with a downlooking oriented HR ADCP mounted on a V4 SWIFT drifter. Profiles span a period of 4 seconds, and line color indicates the relative timing of each profile. Strong profile-scale background shear due to wave orbital velocities is apparent in the profiles, superimposed with fine-scale turbulent fluctuations.

Example profiles of along-beam velocity measured by the ADCP showcase the superposition of wave orbital velocities and turbulence in the data (Figure 2). Velocities increase with distance from the platform as the SWIFT buoy moving with the waves at the surface. Wave velocities dominate the profiles, and it is clear that calculating $D(z,r)$ prior to filtering out wave shear would result in bias with increasing severity towards the surface. As $D(z,r)$ is a positive definite quantity, wave bias will produce stronger than actual $\epsilon(z)$. We expect low-mode EOFs to reflect the profile shape (i.e. shear) and variability of these wave velocities, with no variance at turbulent scales.

C. Synthetic Wave Data

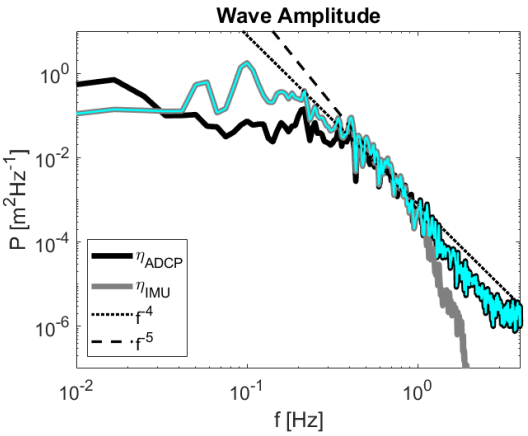

Fig. 3. Surface gravity wave spectrum measured by the SWIFT used to generate synthetic wave data (cyan). The spectrum is a composite of the surface elevation spectrum derived from the onboard IMU vertical acceleration (grey), and from vertical velocity measured by at the deepest ADCP bin (black line). Above 1 Hz, the IMU spectra are damped by the SWIFT motion so the ADCP data are used to create an artificial tail.

Synthetic wave data were generated using surface gravity wave spectra concurrently measured by the SWIFT (Figure 3). We obtain surface elevation by double integrating vertical acceleration measured by the onboard IMU as part of a GPS-aided motion solution with an extended Kalman filter (EKF) (grey line). The resultant wave spectrum follows f^{-4} below the peak frequency as expected for waves in local equilibrium with the wind [9]. However the spectrum is damped below 1 Hz, the natural frequency of the buoy. To obtain a full wave spectrum, we construct an artificial 'tail' using the ADCP data. We estimate vertical displacement by integrating relative vertical velocity in the deepest ADCP bin, which we expect to most closely reflect the true wave velocity at the surface (black line, recall the ADCP measures velocity with respect to the buoy motion). The resultant spectral tail follows f^{-5} as expected for high-frequency wind-waves which dissipate locally [10]. A composite spectrum is then constructed by combining the IMU spectrum below 1 Hz with the ADCP spectrum above 1 Hz. Individual wave components are computed for the full depth range of the ADCP and over a burst using the equation for linear surface gravity waves

$$w(z,t) = -\omega A_\omega e^{kz} \cos \omega t + \phi_\omega \tag{3}$$

where $\omega = 2\pi f$ is the component frequency, $k = \omega^2/g$ is the corresponding wavenumber, A_ω is the component amplitude given by the spectrum and ϕ_ω is a random phase. All wave components are superimposed to create a single wave profile at each time-step. Finally we project the synthetic wave velocities into a Lagrangian frame of reference by subtracting the velocity at $z = 0$, to reflect motion of the SWIFT with the waves at the surface and obtain relative velocity.

IV. Results

A. EOF Validation

The purpose of comparing EOFs of the measured ADCP data with those of the synthetic, wave-only data is to demonstrate that the low-mode EOFs which were attributed to surface gravity waves by [2] are indeed representative of waves and do not contain any variance attributable to turbulence. In other words, the goal is to confirm that removing low-mode EOFs from the data sufficiently removes wave velocities and does not also remove turbulent shear from the data prior to computing $\epsilon(z)$ (which would lead to an underestimate). If low-mode EOFs of the data exhibit characteristics of surface gravity waves, they can be used to construct empirical wave-profiles and filtered from the data.

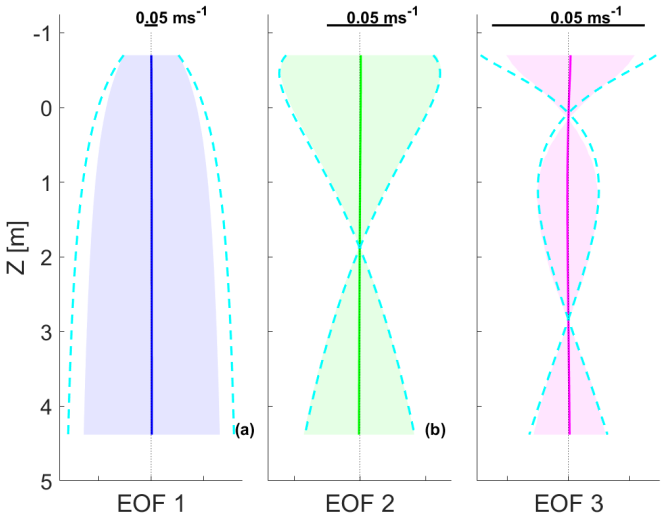

Fig. 4. First three EOFs of the real and wave-only synthetic ADCP data (shaded and dotted lines, respectively). The structure of each EOF is illustrated using bounds given by its depth-dependent variance. The horizontal black line over each EOF is 0.05 ms^{-1} long to indicate the changing magnitude of the variance.

Low-mode EOFs of the two datasets are in tight agreement, as expected. Figure 4 compares the first three EOFs of the real and synthetic data. Shaded regions give the variance of the real data EOFs, while the overlaid dotted cyan lines give the variance of the synthetic data EOFs. There is an order of magnitude difference between the variance of the first EOF and the next two EOFs, indicated by the changing scale of the horizontal black bar above each (equivalent to 0.05 ms^{-1}). The first EOF of both datasets strongly reflects the profile-scale wave shear apparent in Fig. 2. EOF 1 of the real data contains 97% of its total variance, while EOF 1 of the synthetic data contains 99% of its variance. EOFs 2 and 3 reflect the superposition of waves close to the peak frequency but with a phase offset, a consequence of the broadband nature of the wave field in both the real and synthetic data. Importantly, removal of even just the first EOF would remove 99% of the wave energy from the synthetic data (as it only contains waves). Removal of three EOFs from the real data similarly removes 99% of the wave energy.

A key result of [2] was that higher-mode EOFs had characteristics of turbulence. The wavenumber spectra of individual high-mode EOFs were characterized by broadband peaks at successively higher frequencies but with decreasing energy, such that they etched out the characteristic $k^{-5/3}$ slope expected of inertial subrange turbulence (see their Figure 4). Higher-mode EOFs of the synthetic data do not exhibit the same characteristics, as the data does not contain turbulence (Figure. 5). Instead, wavenumber spectra are characteristic of noise. There is comparatively no energy contained in the higher-mode EOFs (note the 20 orders of magnitude range) and their spectra are effectively flat. It is clear the spectral characteristics observed by [2] are due to turbulence in the real data which is absent from the synthetic data.

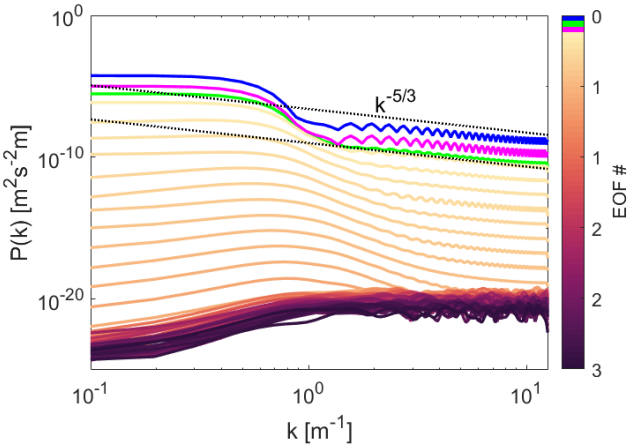

Fig. 5. Wavenumber spectra of the synthetic EOFs. The first three EOFs are colored as in Fig. 4, while higher-mode EOFs are colored in yellow-maroon. Higher-mode spectra are characteristic of noise, as the synthetic data does not contain turbulence.

B. Dissipation Rate Estimates

Here we briefly review the main result of [2]. If computed prior to EOF-filtering the data, $\epsilon(z)$ follows a z^{-2} decay profile (Figure. 6, solid-grey and dotted grey lines, respectively). After filtering, $\epsilon(z)$ is an order of magnitude weaker near the surface and decays as z^{-1}, in tight agreement with the law-of-the-wall scaling prediction derived from concurrent wind speed measurements (red and grey-dashed lines, respectively). We note the filtered estimate diverges from law-of-the-wall scaling in the upper three ADCP bins, giving the appearance of 'elevated' ϵ very close to the surface, to be addressed in the next section. As noted by [2], wave breaking was not observed at this time. The success of law-of-the-wall is expected in this case and provides confidence our estimate of $\epsilon(z)$ is unbiased (below $\sim$ 0.5 m depth).

C. Quantified Wave Bias

The isolated wave profiles may now be used to quantify potential bias due to surface gravity waves (i.e. by computing $\epsilon(z)$ from the filtered-out wave profiles). Profiles of wave bias estimated from the real and synthetic data are in strong

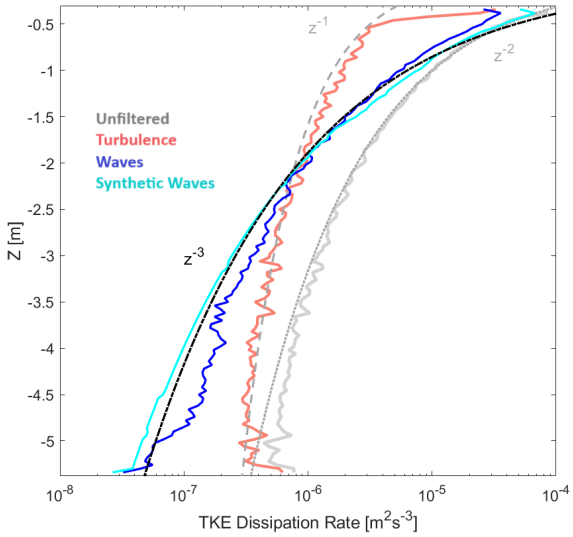

Fig. 6. Profiles of dissipation rate $\epsilon(z)$ computed from the unfiltered data (solid grey line), EOF-filtered data (i.e. turbulent velocities, solid red line), the filtered-out wave profiles (blue line) and the synthetic wave profiles (cyan line). The latter two quantify the wave bias in $\epsilon(z)$ if wave shear is not sufficiently removed from the data. Also shown are the law-of-the-wall prediction for $\epsilon(z)$ which follows z^{-1} (grey dashed line), as well as decay profiles corresponding to z^{-2} (grey dotted line) and z^{-3} (black dashed line). The unbiased estimate of $\epsilon(z)$ closely follows the law-of-the-wall scaling, while wave bias is an order of magnitude stronger at the surface and decays as z^{-3}.

agreement, lending further confidence in the EOF-filtering technique (Fig. 6, blue and cyan lines, respectively). Wave bias is an order of magnitude stronger than the true dissipation rate at the top of the profile, and decays as $\sim z^{-3}$ (dashed-black line). We note wave-bias computed from the real data is a few times weaker than the synthetic data in the upper few ADCP bins, actually approaching the filtered $\epsilon(z)$ values in those bins. The comparison with the bias derived from synthetic wave data makes it clear that the apparent 'elevated' dissipation in the upper few bins is actually an artifact of retained wave bias. This reveals a limitation of the EOF-filtering technique in separating turbulence from waves in the upper few bins, likely due to the decreasing scale of wave-shear towards the surface (i.e. approaching turbulence scales).

D. Discussion

In the example above, the agreement of $\epsilon(z)$ with law-of-the-wall scaling is compelling evidence that our results are unbiased. The law-of-the-wall prediction is derived by assuming TKE dissipation is balanced by shear production near the surface, within a layer of constant turbulent stress proportional to the wind stress. Subsequent scaling gives

$$\epsilon(z) = (\rho' u_*)^3 / kz \tag{4}$$

where ρ' is the square root of the ratio of air to water densities ($\sqrt{\rho_a/\rho_w}$), u_* is the air-side friction velocity, k is the Kolmogorov constant and z is vertical distance from the surface. There is clear observational support for law-of-the-wall scaling in the ocean during calm conditions and

under ice where surface waves are significantly damped (e.g. [11], [12]). However, previous observational studies have often found $\epsilon(z)$ elevated with respect to law-of-the-wall scaling under stronger forcing conditions (e.g. [13]–[16]). The widely accepted explanation is that wave breaking drives intense mixing at the surface, subsequently elevating dissipation rates. Most studies have found wave-driven $\epsilon(z)$ to be 1-2 orders of magnitude greater than law-of-the-wall within about a significant wave height from the surface and with a decay rate of $\sim z^{-2}$, although there is a significant degree of variability across observations.

Our results quantifying potential wave bias in $\epsilon(z)$ challenge this interpretation. Note that bias due to background *non-turbulent wave shear* being retained in the data is distinct from the concept of wave-driven *elevated dissipation*, i.e. due to real turbulence which is driven by wave breaking. The profile of dissipation rate computed from the unfiltered data is suspiciously similar to prior observations of 'elevated' wave-driven $\epsilon(z)$ (Fig. 6, solid grey line). This result suggests prior observations may be in all or in part due to underappreciated wave bias. This inference is reinforced by (EOF-filtered) dissipation rate estimates during a storm with peak 10-m wind speeds of 15 ms^{-1} (Figure. 7). In addition to dissipation rate (middle), the air-side friction velocity derived from wind speed measure by the SWIFT (top, black line) and acoustic backscatter amplitude (bottom) are shown for context. Significant wave height is overlaid in black on $\epsilon(z,t)$ and acoustic backscatter to indicate the expected minimum depth of wave-breaking effects. To compare our observations with law-of-the-wall predictions, we invert (4) to obtain $u_*(t)$ from $\epsilon(t)$ (pink line). We have limited the calculation to 0.5-2.5 m depth to avoid the known wave-bias above 0.5 m and a hard-body interference at $\sim$ 3 m depth which occurred late in the record. The u_* comparison implies that the observed dissipation rates closely follow law-of-the-wall scaling, even though there was strong wave-breaking during the storm (confirmed with concurrent images obtained from a camera on the SWIFT). Wave effects were expected down to about 4 m depth at the storm peak, consistent with elevated acoustic backscatter during the storm which implies bubble plumes extended to at least the base of the profile.

There are three plausible explanations for the discrepancy between our results, which show strong adherence to law-of-the-wall scaling for dissipation rates during a storm, and the literature which has found 'elevated' dissipation in the presence of breaking waves. First, as discussed above results from previous studies may contain underappreciated wave bias, as suggested by quantification of wave bias in our analysis. Second, there may be systematic bias in our results due to processing errors or data quality. The synthetic wave analysis suggests that EOF filtering at most *insufficiently* removes wave bias very close to the surface, so it is unlikely excess dissipation is being removed during filtering. However, it is possible strong downwelling during wave breaking events causes excessive spiking in the pulse-coherent data, and these ADCP pings are thus selectively removed during quality

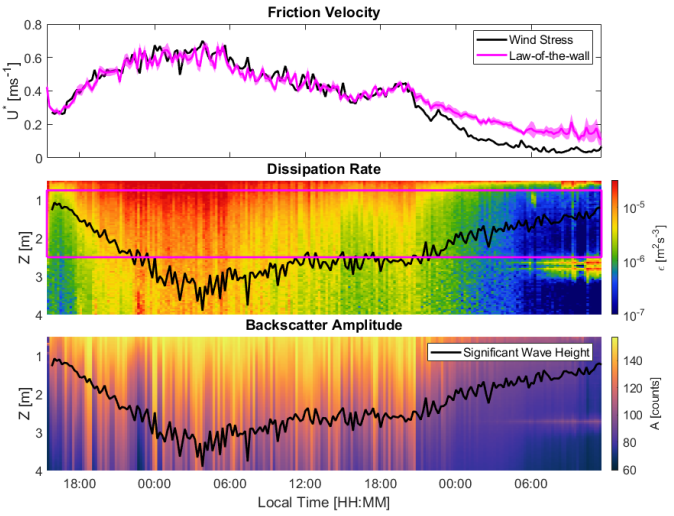

Fig. 7. EOF-filtered dissipation rate estimates during a storm with strong wave breaking. Shown are (top, black line) air-side friction velocity derived from near-surface wind speed, (middle) dissipation rate and (bottom) acoustic backscatter amplitude. Significant wave height is overlaid in black on the latter two to indicate the expected minimum depth of wave effects. Friction velocity derived from the observed dissipation rate by inverting (4), i.e. law-of-the-wall scaling, is in close agreement with the observed friction velocity (pink line). The pink box overlaid on dissipation rate indicates the depth range used to make the comparison. This result is surprising as wave effects reach down to at least 4 m, evident in increased acoustic backscatter indicative of bubble plumes.

control. In a similar fashion, high-void fraction bubble clouds generated at the instance of breaking may cause occlusion of the most intense wave-driven turbulence [17]. We note a preliminary review of the data does not suggest obvious systematic removal of the data or frequent occlusion.

A third likely contribution to variability in observed $\epsilon(z)$ is that differences in sampling methods and indiscriminate averaging in across these studies obscures the role of intermittency. Laboratory and a limited few high-resolution (i.e. wave phase resolved) observational studies have found $\epsilon(z)$ can vary up to a few orders of magnitude from the instant of breaking to even a few seconds later, i.e. that wave-driven 'elevated' dissipation is highly intermittent and decays rapidly in time (exemplified by [18]). Similar intermittency was observed with SWIFT drifters by [16], though crucially that study did not account for wave-shear and those results are almost certainly biased in light of the results presented here and in [2]. Many previous studies attempting to scale 'elevated' dissipation near the surface average observations on timescales of hours or longer. A recent numerical study by [19] found that a Lagrangian platform such as the SWIFT drifter would need to sample for 1000 times the peak wave period to avoid underestimating wave-driven mixing. Peak wave periods during the observations in Fig. 7 were $\sim$ 10 s, corresponding to a minimum sampling period of $\sim$ 2.7 hours, on par with the timescale of variability of the wind speed. However, the storm lasted $\sim$ 18 hours so we may still have expected to see 'elevated' ϵ.

V. Summary and Conclusion

In this study we have used synthetic wave data to validate the EOF-filtering technique of [2]. The low-mode EOFs of both the HR ADCP data and synthetic wave data reflect surface gravity waves, while only the weaker (higher-mode) EOFs of the real data reflect turbulence. We have shown low-mode EOFs can be filtered from the data to produce largely unbiased estimates of near-surface dissipation. We have quantified the potential for wave bias by computing $\epsilon(z)$ from the filtered wave profiles, which demonstrate a striking similarity to results in the literature showing 'elevated' near-surface dissipation attributed to wave breaking. Application of our methodology to turbulent velocity data obtained with a SWIFT drifter during a strong storm reinforces the interpretation that stronger than law-of-the-wall dissipation rates reported in the literature may in part result from underappreciated wave bias. However, intermittency may also play a role in obscuring strong $\epsilon(z)$, and may have prevented convergence on a universal scaling which accounts for enhanced mixing driven by wave breaking.

To disentangle the influences of wave bias and wave-breaking intermittency on scalings for near-surface $\epsilon(z)$, future studies are needed which expand upon the results of [18] and [16], measuring near-surface turbulence in the presence of breaking waves at high temporal resolutions and with robust removal of wave velocities to eliminate bias. Further development of the methodology of [2] is also needed to investigate possible systematic bias towards non-breaking conditions. Currently a limitation of the EOF-filtering method is the subjective choice of which number of low-mode EOFs to use in the reconstruction. Expansion of the synthetic wave data analysis, combined with a sensitivity analysis, to wider dataset with a broad range of forcing conditions would help determine an appropriate cutoff empirically. Such a study should additionally explore any parametric dependence of the EOFs on wind and wave state variables.

Acknowledgment

The authors thank APL-UW engineers Alex de Klerk and Joe Talbert for preparation and maintenance of SWIFT buoys across all projects. We also thank the captain and crew of the R/V Sproul who enabled and assisted in deployment and recovery of the SWIFT drifters. Data collection was conducted with funding under Naval Sea Systems Command (NAVSEA) contract N0002419F8705.

References

[1] B. D. Scannell, T. P. Rippeth, J. H. Simpson, J. A. Polton, and J. E. Hopkins, "Correcting surface wave bias in structure function estimates of turbulent kinetic energy dissipation rate," *Journal of Atmospheric and Oceanic Technology*, vol. 34, pp. 2257–2273, 2017.

[2] K. Zeiden, J. Thomson, and J. Girton, "Estimating profiles of dissipation rate in the upper ocean from acoustic doppler measurements below surface following platforms," *J. Amtos. Oceanic. Technol.*, vol. 40, pp. 1571–1589, 2023.

[3] J. Thomson, "Wave breaking dissipation observed with SWIFT drifters," *Journal of Atmospheric and Oceanic Technology*, vol. 29, no. 12, pp. 1866–1882, 2013/01/03 2012. [Online]. Available: https://doi.org/10.1175/JTECH-D-12-00018.1

[4] A. E. Gargett, "Velcro measurement of turbulence kinetic energy dissipation rate," *J. Atmos. Ocean. Tech.*, vol. 16, no. 12, pp. 1973–1993, 1999.

[5] P. Wiles, T. P. Rippeth, J. Simpson, and P. Hendricks, "A novel technique for measuring the rate of turbulent dissipation in the marine environment," *Geophys. Res. Let.*, vol. 33, p. L21608, 2006.

[6] W. Emery and R. Thomson, *Data Analysis Methods in Physical Oceanography: Third Edition*, 01 2004, vol. 80, p. 638.

[7] J. Thomson, M. Moulton, A. de Klerk, J. Talbert, M. Guerra, S. Kastner, M. Smith, M. Schwendeman, S. Zippel, and S. Nylund, "A new version of the swift platform for waves, currents, and turbulence in the ocean surface layer," in *IEEE/OES Workshop on Currents, Waves, and Turbulence Measurements*, March 2019.

[8] A. Y. Shcherbina, E. D'Asaro, and S. Nylund, "Observing finescale oceanic velocity structure with an autonomous nortek acoustic doppler current profiler," *Journal of Atmospheric and Oceanic Technology*, vol. 35, no. 2, pp. 411–427, 2018. [Online]. Available: https://doi.org/10.1175/JTECH-D-17-0108.1

[9] O. Phillips, "Spectral and statistical properties of the equilibrium range in wind-generated gravity waves," *Journal of Fluid Mechanics*, vol. 156, pp. 505–531, 1985.

[10] M. L. Banner, "Equilibrium spectra of wind waves," *Journal of Physical Oceanography*, vol. 20, pp. 966–984, 1990.

[11] A. Perlin, J. N. Moum, J. M. Klymak, M. D. Levine, T. Boyd, and P. M. Kosro, "A modified law-of-the-wall applied to oceanic bottom boundary layers," *Journal of Geophysical Research Letters*, vol. 110, p. C10S10, 2005.

[12] Y. Kawaguchi, Z. Koenig, D. Nomura, M. Hoppmann, J. Inoue, Y. Fang, K. Schulz, M. Gallagher, C. Katlein, M. Nicolaus, and B. Rabe, "Turbulent mixing during late summer in the ice–ocean boundary layer in the central arctic ocean: Results from the mosaic expedition," *Journal of Geophysical Research: Oceans*, vol. 127, p. e2021JC017975, 2022.

[13] E. Terray, M. Donelan, Y. Agrawal, W. Drennan, K. Kahma, A. Williams, P. Hwang, and S. Kitaigorodskii, "Estimates of kinetic energy dissipation under breaking waves," *J. Phys. Oceanogr.*, vol. 26, pp. 792–807, 1996.

[14] A. Soloviev and R. Lukas, "Observation of wave-ehanced turbulence in the near-surface layer of the ocean during TOGA COARE," *Deep-Sea Research I*, vol. 50, pp. 371–395, 2003.

[15] G. Gerbi, J. Trowbridge, E. Terray, A. J. Plueddemann, and T. Kukulka, "Observations of turbulence in the ocean surface boundary layer: energetics and transport," *J. Phys. Oceanogr.*, vol. 39, pp. 1077–1096, 2009.

[16] J. Thomson, M. S. Schwendeman, S. F. Zippel, S. Moghimi, J. Gemmrich, and W. E. Rogers, "Wave-breaking turbulence in the ocean surface layer," *Journal of Physical Oceanography*, vol. 46, no. 6, pp. 1857–1870, 2016. [Online]. Available: http://dx.doi.org/10.1175/JPO-D-15-0130.1

[17] G. Deane, "The performance of high-frequency doppler sonars in actively breaking wave crests," *IEEE Journal of Oceanic Engineering*, vol. 41, no. 4, pp. 1028–1034, 2016.

[18] J. R. Gemmrich and D. Farmer, "Near-surface turbulence in the presence of breaking waves," *J. Phys. Ocean.*, vol. 34, pp. 1067–1086, 2004.

[19] M. Derakhti, J. Thomson, and J. T. Kirby, "Sparse sampling of intermittent turbulence generated by breaking surface waves," *Journal of Physical Oceanography*, vol. 50, no. 4, pp. 867–885, 2020.